Structure, compressibility, hydrogen bonding, and dehydration of the tetragonal Mn^{3+} hydrogarnet, henritermierite

THOMAS ARMBRUSTER,[1,*] THOMAS KOHLER,[1] EUGEN LIBOWITZKY,[2] ALEXANDRA FRIEDRICH,[3]
RONALD MILETICH,[3] MARTIN KUNZ,[3] OLAF MEDENBACH,[4] AND JENS GUTZMER[5]

[1]Laboratorium für chemische und mineralogische Kristallographie, University of Bern, Freiestrasse 3, CH-3012 Bern, Switzerland
[2]Institut für Mineralogie und Kristallographie, Universität Wien–Geozentrum, Althanstrasse 14, A-1090 Vienna, Austria
[3]Laboratory of Crystallography, ETH Zentrum, CH-8092 Zürich, Switzerland
[4]Institut für Mineralogie, Ruhr-Universität Bochum, Germany
[5]Department of Geology, Rand Afrikaans University, P.O. Box 524, Auckland Park 2006, South Africa

ABSTRACT

Henritermierite, space group $I4_1/acd$, at 293 K $a = 12.489(1)$, $c = 11.909(1)$ Å, $Z = 8$, with close to end-member composition $(Ca_{2.98}Na_{0.01}Mg_{0.01})^{VIII}(Mn_{1.95}Fe_{0.01}Al_{0.04})^{VI}[SiO_4]_{2.07}[H_4O_4]_{0.93}$ from the N'Chwaning II mine at the Kalahari manganese fields, Republic of South Africa, has been studied by single-crystal X-ray diffraction at 100 and 293 K at ambient pressure and up to 8.7 GPa in a diamond-anvil cell at 293 K. Polarized FTIR spectroscopy at 80 and 293 K was also performed. The Mn$^{3+}O_6$ octahedra display a tetragonally elongated type of Jahn-Teller distortion where the oxygen atoms of the elongated O-Mn-O axis (Mn-O: 2.2 Å) are moderately hydrogen bonded (O-H···O: 2.76 Å) to the H_4O_4 tetrahedra, which replace 1/3 of SiO_4 tetrahedra in an ordered fashion. Thus Jahn-Teller distortion and H_4O_4 arrangement are coupled and both are responsible for the tetragonal bulk symmetry. The H_4O_4 tetrahedra have a center-to-O distance of 1.98 Å and the H atoms are slightly above the tetrahedral faces as similarly observed in the synthetic katoite end-member, $Ca_3Al_2[H_4O_4]_3$. However, in henritermierite the O-H···O hydrogen bond is considerably bent (ca. 131°) and gives rise to an OH stretching mode at 3432(5) cm^{-1}. Additional, though weak, IR absorptions at 3508(2) and 3553(2) cm^{-1} may be due to more remote hydrogen-bond acceptors (O-H···O: 3.29 Å) within the H_4O_4 tetrahedra.

Compressibility data for a third-order Birch-Murnaghan equation of state yield a bulk modulus of $K_0 = 97.9(9)$ GPa with a pressure derivative of $K' = 5.3(3)$. The axial compressibilities indicate a pronounced compressional anisotropy which is explained by the orientation of the elongated axes of the Jahn-Teller distorted MnO$_6$ octahedra along the slightly more compressible $[100]_{tetr}$ directions compared to the c-axis. The crystal structure was refined at a pressure of 8.6 GPa. The MnO$_6$ octahedra were observed to show anisotropic compression towards a more isometric shape. Calculated spontaneous strain reveals a trend towards a weaker tetragonal distortion.

If henritermierite is heated above 800 K in air it dehydrates and Mn^{3+} is partially oxidized to Mn^{4+}. This topotactic transformation leads to a new garnet-like phase of $Ia3d$ symmetry with $a = 12.12$ Å and of $Ca_3Mn_{2.26}O_{2.32}[SiO_4]_{2.42}$ composition in which instead of H_4O_4 tetrahedra a new disordered octahedral site is occupied by Mn.

INTRODUCTION

Henritermierite is a rare Mn^{3+} silicate belonging to the hydrogarnet group of minerals. There are two occurrences, both in manganese mines, one at Tachgagalt, Anti-Atlas Mountains, Morocco (Gaudefroy et al. 1969), and the other at the N'Chwaning and Wessels mine, Kalahari manganese fields, Republic of South Africa, (Cairncross et al. 1997 and references therein).

End-member henritermierite has the formula $Ca_3Mn_2^{3+}[SiO_4]_2[OH]_4$. Due to the Jahn-Teller distortion of octahedral Mn^{3+} henritermierite is tetragonal (space group $I4_1/acd$) which is in contrast to other hydrogarnets of the hibschite and hydroandradite series (e.g., Kobayashi and Shoji 1987; Armbruster and Lager 1989; Lager et al. 1989; Armbruster 1995). It is believed that henritermierite from the Kalahari manganese field is a hydrothermal reaction product of the original braunite-rich manganese ores (Cairncross et al. 1997). Corresponding formation conditions have been proposed for the Morocco sample (Gaudefroy et al. 1969). At Tachgagalt henritermierite has substantial octahedral Al, whereas in the Kalahari manganese fields it occurs with nearly end-member composition.

In general, Mn^{3+}-rich garnets are rather rare in nature. $Ca_3Mn_2^{3+}[SiO_4]_3$ and $Cd_3Mn_2^{3+}[SiO_4]_3$ were synthesized by Nishizawa and Koizumi (1975) at 1100 °C between 3 and 6 GPa and synthetic high-pressure $Mn_3Mn_2^{3+}[SiO_4]_3$, produced at

1000 °C and 9 GPa, was recently reinvestigated by Arlt et al. (1998). The latter garnet is known as "blythite" component, e.g., observed in natural calderite-andradite (Bühn et al. 1995). Surprisingly, the synthetic Mn^{3+}-silicate garnets were found to have cubic symmetry (space group $Ia3d$). Arlt et al. (1998) showed that a disordered Jahn-Teller distortion, either of dynamic or static nature, must be assumed for $Mn_3Mn_2^{3+}[SiO_4]_3$. In contrast, the synthetic germanate garnet $Ca_3Mn_2^{3+}[GeO_4]_3$ (Heinemann and Miletich 2000) is tetragonal (space group $I4_1/a$) at room temperature but becomes cubic (space group $Ia3d$) at ~800 K.

Holstam and Hålenius (1998) recorded the optical absorption spectrum of henritermierite and found four Gaussian-shaped bands in both principal vibration directions at 23 000, 21 300, 19 600, and 12 200 cm^{-1}. This is consistent with transitions expected for $Mn^{3+}O_4(OH)_2$ octahedra. Calculated values for Δ_0 and crystal-field stabilization energies are 15 200 cm^{-1} and 182 kJ/mol, respectively. Optical absorption spectra of other synthetic and natural Mn^{3+}-bearing garnets of cubic symmetry have been reported by Frentrup and Langer (1981), Langer and Lattard (1984), Amthauer et al. (1989), and Geiger et al. (1999).

Hydrogarnets are known as solid-solution series between grossular $Ca_3Al_2[SiO_4]_3$ and katoite $Ca_3Al_2[H_4O_4]_3$ (e.g., Sacerdoti and Passaglia 1985, Armbruster and Lager 1989, Lager et al. 1989) and between andradite $Ca_3Fe_2[SiO_4]_3$ and $Ca_3Fe_2[H_4O_4]_3$ (e.g., Kobayashi and Shoji 1987; Armbruster 1995). These minerals are cubic and the structure of intermediate members reveals a disordered distribution of small SiO_4 tetrahedra and larger H_4O_4 tetrahedra. The H atoms of the H_4O_4 tetrahedron are approximately on the tetrahedral faces. A very low degree of hydrogarnet substitution is known for many natural garnets (Aines and Rossman 1984). Titanian andradites with the morimotoite substitution $Fe^{2+} + Ti^{4+} \rightarrow 2 Fe^{3+}$ (Henmi et al. 1995) are characterized by a substantial hydrogarnet substitution reducing structural strain (Armbruster et al. 1998). In contrast to the disordered arrangement of H_4O_4 in hydrogarnets related to grossular and andradite, henritermierite has ordered H_4O_4 units (Aubry et al. 1969). The additional Mn^{3+} Jahn-Teller distortion in henritermierite could be responsible that an ordered arrangement of small SiO_4 and large H_4O_4 tetrahedra is more favorable to compensate for the ordered octahedral distortion. The single-crystal X-ray diffraction structure study by Aubry et al. (1969) of an Al-rich henritermierite from Morocco could not resolve the hydrogen distribution.

Because garnets are assumed to be possible hosts for the storage of water in the Earth's mantle, many studies have dealt with the high-pressure behavior of garnets. Previous work on the compressibility of the cubic end-members of the garnet-hydrogarnet series grossular $Ca_3Al_2[SiO_4]_3$ – katoite $Ca_3Al_2[H_4O_4]_3$ concentrated on the influence of the hydrogarnet substitution. Lager and von Dreele (1996) reported the behavior of the D_4O_4 groups of deuterated katoite as a function of pressure. The behavior of manganese rich garnets was investigated under high pressure for spessartine, $Mn_3Al_2[SiO_4]_3$ (Babuska et al. 1978; Leger et al. 1990), $Mn_3^{2+}Mn_2^{3+}[SiO_4]_3$ (Arlt et al. 1998), and for tetragonal $Ca_3Mn_2^{3+}[GeO_4]_3$ (Miletich et al. 1997).

The goals of this study are manifold. (1) An accurate struc-

tural investigation of close to end-member henritermierite at low and ambient temperature should resolve the hydrogen bonding in this garnet. (2) Polarized Fourier Transform Infrared (FTIR) spectroscopy at low and ambient temperature is applied to correlate the structurally determined H positions with spectroscopic results. (3) High-pressure single-crystal X-ray diffraction is used to determine the compressibility of this hydrogarnet. (4) High temperature dehydration and oxidation is studied by single-crystal X-ray methods to analyze the decomposition product.

EXPERIMENTAL METHODS

Sample description

The sample material comes from the N'Chwaning II mine, Kalahari manganese ore fields, RSA. Euhedral crystals of henritermierite (up to 10 mm in diameter) studied usually resemble octahedra with curved faces. This shape is actually composed by a threefold axial twin around ~[111] with the forms {221}, the "octahedron", and {112}, the truncated corners of the "octahedron" (Fig. 1). Smaller henritermierite crystals, e.g., displayed by Cairncross et al. (1997), have smooth {111} faces and show no indication of twinning. Due to the similar orange color and crystal form, henritermierite and hydrous Mn-bearing andradite (Armbruster 1995) can easily be confused.

Electron microprobe analysis

Chemical analyses were performed on a Cameca CAMEBAX 355 electron-microprobe system equipped with a Link energy dispersive spectrometer (EDS), carrying a Li-doped Si-detector, at the Department of Geology, Rand Afrikaans University. The system was controlled by the Link ExL II and Lemas software packages. The raw EDS spectra were automatically ZAF-corrected by the ExL II software. Data were obtained from one polished, carbon-coated section of henritermierite. The electron beam was set for all analyses at 15 kV acceleration voltage and 10 nA absorbed beam current on brass. Routine calibration of the EDS was performed using a pure Co metal standard. The quality of the analyses was ascertained by analyzing an almandine standard before and after the set of 16 analyses of henritermierite. Spectra for standard and sample were acquired for 100 s.

Single-crystal X-ray measurements at ambient conditions and at 100 K

A small untwinned crystal fragment, translucent orange brown in color, was separated from a larger crystal and studied with a single-crystal X-ray diffractometer at room temperature (293 K) and at 100 K using a conventional liquid nitrogen cooling device. Cell dimensions were refined from the angular settings of 24 reflections with $27 < \theta < 41°$ yielding tetragonal symmetry. Experimental details are given in Table 1. Data reduction, including background and Lorentz polarization correction, was carried out with the SDP program system (Enraf Nonius 1983). An empirical absorption correction using the ψ-scan technique was applied. Systematic absences confirmed the space group $I4_1/acd$. Structure solution and refinement were performed with neutral-atom scattering factors and the programs

TABLE 1. Data collection and refinement parameters of henritermierite

Crystal size (mm³)	$0.1 \times 0.2 \times 0.175$		$0.1 \times 0.05 \times 0.08$
Diffractometer	Enraf Nonius CAD4		Siemens Smart
X-ray power	55 kV, 32 mA		50 kV, 40 mA
Temperature	100 K	293 K	293 K*
Reflections measured	2226	4235	2296
max. θ	40	40	27.1
Unique reflections > 2σ(I)	1179	1167	99
Space group	$I4_1/acd$ (No. 142)	$I4_1/acd$ (No. 142)	$Ia3d$ (no. 230)
cell dimensions (Å)	$a = 12.468(1)$	$a = 12.489(1)$	$a = 12.1225(9)$
	$c = 11.894(2)$	$c = 11.909(1)$	
R(int) after empirical absorption correction	2.91%	2.64%	12.4%
$R(\sigma)$	2.68%	1.63%	4.7%
Number of l.s. parameters	59	59	20
GooF	1.166	1.224	1.721
$R1$, $F_o > 4\sigma(F_o)$	1.82%	1.62%	4.02%
$wR2$ (on F^2)	4.92%	3.90%	9.89%

Note: F_o: observed structure factor, F_c: calculated structure factor
$R(int) = \Sigma \mid F_o^2 - F_o^2(mean) \mid / \Sigma [F_o^2]$.
$R(\sigma) = \Sigma [\sigma(F_o^2) / \Sigma [F_o^2]$.

$$R1 = \left(\sum \| F_o \mid - \mid F_c \| \right) / \left(\sum \mid F_o \mid \right), \ wR2 = \sqrt{\left(\sum w \left(F_o^2 - F_c^2 \right)^2 \right) / \left(\sum w \left(F_o^2 \right)^2 \right)}.$$

$$GooF = \sqrt{\left(\sum w \left(F_o^2 - F_c^2 \right)^2 \right) / (n - p)}$$

n = number of F, p = number of l.s. parameters.
$w = 1 / [\sigma2(F_o^2) + (0.017 P)^2 + 1.0 P]$ where $P = [Max (F_o^2, 0) + 2 F_c^2] / 3$.
In all cases, X-ray radiation was sealed tube Mo$K\alpha$, graphite monochromatized.
* After heating to 800 K.

SHELXS-97 and SHELXL-97 (Sheldrick 1997). Test refinements indicated a weak electron density peak in the center of the H_4O_4 tetrahedron thus Si (Si2) with variable occupancy was refined on this position. This low Si occupancy also indicated that O3 and H3 can not completely be occupied and an additional low occupied O site (O3A) was refined completing the tetrahedral coordination of Si2. Final residual electron densities for both data sets were ± 0.6 e/Å³. These residual peaks were close to Mn1.

Single-crystal X-ray measurements under high-pressure conditions

Two sets of unit-cell data as a function of pressure with a total of 19 data points were obtained by means of single-crystal X-ray diffraction. An untwinned single-crystal fragment was loaded in an ETH-design diamond-anvil cell (DAC) together with a quartz crystal as internal pressure calibrant (Angel et al. 1997) and a 4:1 methanol-ethanol mixture as hydrostatic pressure-transmitting medium. The diamond anvils had a culet face diameter of 0.6 mm. A 250(5) μm hole was drilled in a steel gasket (pre-indented to a thickness of 90 μm) by electro erosion. The first data set with a $160 \times 140 \times 60$ μm³ crystal was measured to a maximum pressure of 6.9 GPa. A second data set was collected up to 8.7 GPa with a smaller $130 \times 100 \times 35$ μm³ single-crystal fragment. The measurements were performed at room temperature with a HUBER four-circle diffractometer using unfiltered and non-monochromatized Mo X-ray radiation (50 kV, 40 mA). Accurate unit-cell parameters of both the quartz and the garnet crystals were obtained applying the diffracted-beam centering technique (King and Finger 1979) to prevent crystal-offset errors. For garnet, 23–29 accessible reflections with $9.2° \leq 2\theta \leq 25.8°$ were used. Pressure calibration was done with 7–14 quartz reflections with $9° \leq 2\theta \leq 32°$. The lattice parameters constrained to the respective symmetries were
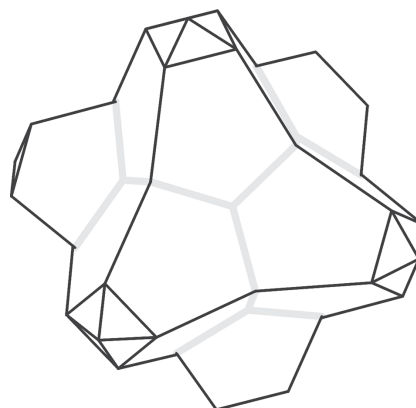

FIGURE 1. Henritemierite, twinned, {112} and {221}. Twinning of macroscopic henritermierite "crystals" resembling octahedra with concave curved faces.

obtained by a vector least-squares fit to the corrected reflection positions.

To obtain compressibilities, P-V, P-a, and P-c data were fitted with a third-order Birch-Murnaghan equation-of-state using a fully weighted least-squares procedure. The pressures were determined from the refined unit-cell parameters and the equation-of-state parameters of quartz (Angel et al. 1997). At the maximum pressures of 8.6 and 8.7 GPa the quartz started to show peak broadening, probably caused by bridging of the diamond anvils by the quartz crystal. Therefore, the last two pressures were derived from the equation of state of henritermierite itself. The slightly different unit-cell parameters

of the two individual crystals of henritermierite at ambient conditions are attributed to small variations of the chemical composition.

X-ray intensity data-collection was performed at 8.6 GPa (at room temperature) with an Enraf Nonius CAD4 four-circle diffractometer with graphite-monochromatized Mo$K\alpha$ radiation (50 kV, 30 mA). The intensity measurements were carried out with ω-scans (max. scan time: 600 s) at the position of least attenuation of the pressure cell, according to the fixed-φ technique (Finger and King 1978) in order to maximize reflection accessibility and minimize attenuation of the X-ray beams by the pressure-cell components. All symmetry-allowed accessible reflections within a full sphere were collected up to $\theta = 35°$ (4565 reflections). Intensity data were obtained from the scan data using a modified Lehmann-Larsen algorithm (Grant and Gabe 1978). Intensities were corrected for Lorentz and polarization effects. Absorption effects of the diamond and beryllium components of the pressure cell were adjusted by a modified version of ABSORB (Burnham 1966). Averaged structure factors were obtained by averaging symmetry equivalent reflections in Laue symmetry 4/*mmm* following the criteria recommended by Blessing (1987).

The structure refinements were carried out with RFINE99 [a modified version of REFINE4 by Finger and Prince (1975)]. The atomic coordinates given from the ambient-condition measurements were used as a starting model. The coefficients for neutral-atom scattering factors and the coefficients for dispersion corrections were taken from the *International Tables for Crystallography* (Maslen et al. 1992; Creagh and McAuley 1992). The final refinements of the high-pressure data set were carried out with anisotropic displacement parameters for the manganese and calcium sites, and isotropic B's for the silicon and oxygen positions. The fractional coordinates and B values of the hydrogen atom and of the low occupied silicon site (Si2) as well as the corresponding occupancies were fixed according to the ambient-condition refinements. The effect of extinction could be neglected and therefore was excluded from refinements to minimize the number of parameters. Few reflections were excluded from refinements according to influences of overlapping diamond reflections as well as of their $\lambda/2$ artifacts and of unreliable integration of weak reflections caused by high and uneven background. Details of the data reduction and refinements are given in Table 2.

Single-crystal X-ray measurements after heating excursion

An additional henritermierite single-crystal was mounted with a temperature resistant sodium-tetrasilicate cement on a quartz glass fiber and was heated in situ (hot-air blower) on a CCD-equipped single-crystal diffractometer. The variation of cell dimensions was subsequently studied as a function of temperature. At ca. 750 K the crystal adopted cubic symmetry with $a = 12.12$ Å. At the same time the single-crystal reflections became strongly streaked along the ω-direction and decreased rapidly in intensity. The cubic symmetry and the streaked reflection characteristics were preserved when the crystal was cooled to room temperature. The original orange-brown crystal turned black and became porous and very fragile. A room-

temperature diffraction data set was subsequently collected and the structure of this dehydrated and partly oxidized garnet-related phase was solved and refined with the program SHELXL-97 (Sheldrick 1997).

Single-crystal IR spectroscopy

A twin crystal, ~4 mm in size, was oriented by the precession method and embedded in epoxy resin. It was cut in 250 µm thick slices parallel to (100) with a low-speed diamond-wheel saw. Thus, the center section contained two twin shares, each with the fourfold axis parallel to the section. The off-center sections contained in addition also the third twin share in isotropic orientation (001). For IR spectroscopy one section was polished on both sides with diamond films to a thickness of 10 µm.

IR spectroscopic measurements were performed on a Perkin Elmer FTIR microscope (6×/0.60 N.A. Cassegrain mirror lenses, liquid nitrogen cooled MCT detector) connected to a Perkin Elmer 1760 X FTIR spectrometer (ceramic globar light source, KBr beam splitter). The sample was mounted on a 400 µm dual aperture (sample aperture vs. empty background aperture) in a Linkam THMS600/FTIR freezing/heating stage. Polarized absorption spectra (KBr gold wire grid-polarizer, extinction ratio 1:100) were acquired between 6000 and 1500 cm⁻¹ with 100 µm effective aperture at 298 and 80 K. Spectra were averaged from 128 single scans at 4 cm⁻¹ resolution. Data processing was managed with the IRDM software package (Perkin Elmer).

Optical measurements

To test for possible low-temperature phase transitions in henritermierite the optical retardation was measured between 80 and 350 K on a doubly polished, 140 µm thick, crystal slab. However, there was no indication of a phase transition and the birefringence increased homogeneously with temperature. The dispersion of accurate refractive indices was measured by the minimum-deviation method from oriented and polished prisms of henritermierite. Experimental details are given in Medenbach and Shannon (1997). At 644 nm, $n_o = 1.7904$, and $n_e = 1.8637$; at 577 nm, $n_o = 1.7982$, and $n_e = 1.8747$; at 546 nm, $n_o = 1.8033$, and $n_e = 1.8823$. Due to strong absorption, refractive indices could not be measured at lower wave lengths. Refractive indices and birefringence of this nearly end-member henritermierite are considerably higher than those [$n_o = 1.765(5)$, $n_e = 1.800(5)$] of the Tachgagalt sample with Ca$_3$(Mn$_{1.5}$Al$_{0.5}$)[SiO$_4$]$_2$[H$_4$O$_4$] composition (Gaudefroy et al. 1969).

RESULTS

The average of 16 point analyses with the electron microprobe (Table 3), normalized to (Al + Fe + Mn + Mg + Ca + Na) = 5, yielded the composition (Ca$_{2.98}$Na$_{0.01}$Mg$_{0.01}$)^{VIII}(Mn$_{1.95}$Fe$_{0.01}$Al$_{0.04}$)^{VI}[SiO$_4$]$_{2.07}$[H$_4$O$_4$]$_{0.93}$ indicating nearly end-member composition. The formula independently refined from X-ray data was Ca$_3$^{VIII}(Mn$_{1.93}$Al$_{0.07}$)^{VI}[SiO$_4$]$_{2.06}$[H$_4$O$_4$]$_{0.94}$.

Refined coordinates of henritermierite and its garnet-like dehydration product are given in Table 4, anisotropic displacement parameters in Table 5[1], selected interatomic distances in Tables 6 and 7, results of bond-valence calculations (Brown

TABLE 2. Details on data reduction and results of the high-pressure structure refinements of henritermierite at 8.7 GPa

Total $|F|$	4565	R_{int} ($F > 4\sigma$)	2.99%
Averaged $|F|$	874	$|F|_{obs}/p_{var}$	6.5
$|F|_{obs}$ ($F > 4\sigma$)	183	R ($F > 4\sigma$)	3.2%
μ (Mo$K\alpha$) (cm⁻¹)	49.02	wR ($F > 4\sigma$)	3.5%
t_{min} (%)	26.2	wR (874)	5.5%
t_{max} (%)	35.4	GooF	1.01

Notes: Transmission (t) includes both crystal absorption and absorption by DAC components. F_o = observed structure factor, F_c = calculated structure factor.

p_{var}= 28.

$R = \left(\sum||F_o|-|F_c||\right)/\left(\sum|F_o|\right)$.

$wR = ((\Sigma w(|F_o|-|F_c|)^2)/(\Sigma w|F_o|^2))^{-1/2}$ and $w = (\sigma^2 + P^2 F_o^2)^{-1}$, $P = 0.016$

$GooF = \sqrt{\left(\sum w\left(F_o^2 - F_c^2\right)^2\right)/(n-p)}$

n = number of F = 874, p = number of l.s. parameters = 28.

TABLE 3. Chemical composition of henritermierite from Tachgagalt (Gaudefroy et al. 1969) and from N'Chwaning II (this paper)

oxide (wt%)	Tachgagalt (Morocco)	Average N'Chwaning II (RSA)	Range N'Chwaning II (RSA)	Atoms pfu N'Chwaning II (RSA)
SiO_2	24.65	26.22	25.87–26.62	2.072
Al_2O_3	5.95	0.48	0.22–0.94	0.045
Fe_2O_3	0.95	0.14	0–0.37	0.008
Mn_2O_3	24.90	32.36	31.53–33.22	1.947
MgO		0.09	0–0.23	0.011
CaO	35.45	35.20	34.17–36.01	2.981
Na_2O		0.06	0–0. 17	0.009
H_2O	7.85	5.46*	4.39–6. 80*	2.878

* H_2O content determined by difference.

1996) in Table 8, and difference mean-square displacement parameters (ΔU) along the Me-O vector (e.g., Armbruster and Geiger 1993) in Table 9.

High-pressure unit-cell parameters of the investigated pressure range of 0.0001 to 8.7 GPa are summarized in Table 10. Because the two crystals differ in V_0 (Table 10), the two sets of P-V data were fitted individually to a third-order Birch-Murnaghan equation-of-state. This results in $K_0 = 97.6(9)$ GPa and $K' = 5.2(3)$ for the first data set and in $K_0 = 98.2(7)$ GPa and $K' = 5.4(2)$ for the second data set. The compressibility values therefore agree within their standard deviations. The averaged bulk modulus and its pressure derivative are $K_{0,T} = 97.9(9)$ GPa and $K' = 5.3(3)$. The averaged axial compressibilities obtained from P-a and P-c data are: a-axis: $K(a)_0 = 256(2)$ GPa [$K(a)_1 = 255.3(2.6)$, $K(a)_2 = 257(2)$], $K(a)' = 17.5(9)$ [$K(a)_1' = 17.3(9)$, $K(a)_2' = 17.6(9)$] and c-axis: $K(c)_0 = 407(5)$ GPa [$K(c)_1 = 408(5)$, $K(c)_2 = 405(4)$], $K(c)' = 13.6(1.5)$ [$K(c)_1' = 12.1(1.5)$, $K(c)_2' = 15.1(1.3)$]. The variation of the normalized unit-cell parameters with pressure can also be described by second-order polynomial equations:

$$a/a_0 = 0.99997(6) \text{ Å} - 3.77(3) \times 10^{-3} \text{ Å GPa}^{-1} \times P + 8.3(4) \times 10^{-5} \text{ Å GPa}^{-2} \times P^2$$

$$c/c_0 = 1.00001(4) \text{ Å} - 2.45(2) \times 10^{-3} \text{ Å GPa}^{-1} \times P + 3.7(3) \times 10^{-5} \text{ Å GPa}^{-2} \times P^2$$

The pressure dependencies of the a- and c-axes are significantly non-linear as indicated by the terms of P^2 being more than 10 times their esds. The fit of a higher order polynomial is not justified as it gives terms of the same magnitude as their uncertainties. These results show a pronounced anisotropy of the axial compression.

Room-temperature polarized IR absorption spectra of henritermierite (Fig. 2) display a smooth, broad absorption band at 3432(5) cm⁻¹. The band parallel to the c-axis is more intense and broader by a factor of 3. At 80 K the bands increase in their peak height and the broad band shape of the $\mathbf{E} \parallel \mathbf{c}$ spectrum becomes well resolved (Fig. 2). The band position is only slightly shifted to 3435(5) cm⁻¹, the two resolved side bands in the $\mathbf{E} \parallel \mathbf{c}$ spectrum occur at 3508(2) and 3553(2) cm⁻¹. The bands are assigned to OH stretching modes of henritermierite. The shallow humps around 3300 cm⁻¹ are caused by interference fringes in the extremely thin and double-sided polished platelet (well visible in the background regions of the spectra outside the depicted range). The tiny spikes in the $\mathbf{E} \parallel \mathbf{c}$ spectra (especially those on top of the main band in the 80 K spectrum) are noise enhanced by the strong absorption that truncates the bands in the 80 K spectra at absorbance ~3 (this is equivalent to transmittance $T = 0.0010(2)$ which is very close to the baseline at $T = 0$).
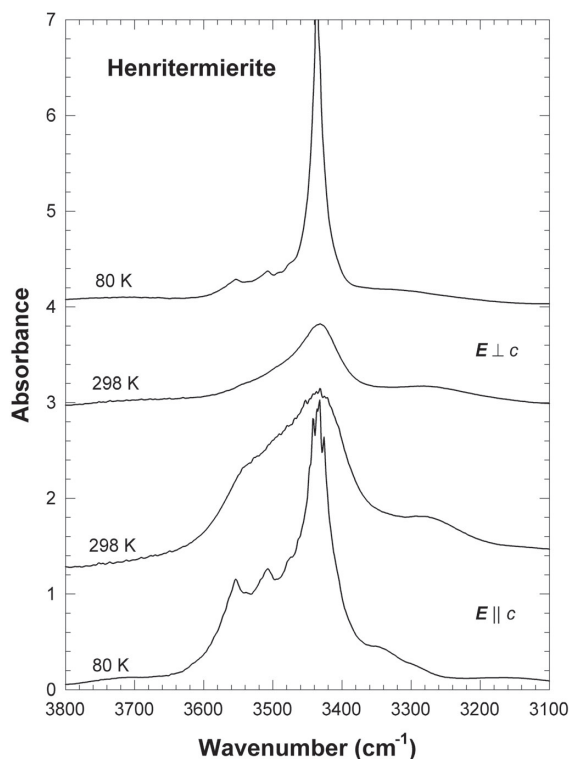

FIGURE 2. Polarized single-crystal IR spectra of henritermierite recorded at 80 and 298 K. Spectra are offset (from bottom to top) by A = 0, 1.2, 3.0, 4.0. Thickness is 10 μm.

TABLE 4. Final atomic coordinates and B_{eq} (Å^2) values, with standard deviations in parentheses, for henritermierite and dehydrated-oxidized henritermierite after heating excursion to 800 K

atom	pop.	x/a	y/b	z/c	B_{eq}
			100 K (space group *I4$_1$/acd*)		
Mn1	0.967(2)†	0	0	0	0.233(3)
Ca1	1.0	0.36177(2)	0	1/4	0.309(3)
Ca2	1.0	0	1/4	1/8	0.352(3)
Si1	1.0	0.11595(3)	0	1/4	0.248(5)
O1	1.0	0.29522(6)	0.71857(6)	0.09654(6)	0.361(8)
O2	1.0	0.15985(6)	0.55463(5)	0.05400(6)	0.387(8)
O3	0.954(5)	0.4427(1)	0.3601(1)	0.0219(1)	0.43(1)
Si2	0.044(4)	1/2	1/4	1/8	0.4(2) *
H3	0.95	0.432(2)	0.350(2)	0.083(2)	2.1(5) *
O3A	0.044	0.454(3)	0.347(3)	0.030(3)	0.79 *
			293 K (space group *I4$_1$/acd*)		
Mn1	0.967(2)†	0	0	0	0.427(2)
Ca1	1.0	0.36180(2)	0	1/4	0.558(3)
Ca2	1.0	0	1/4	1/8	0.673(3)
Si1	1.0	0.11599(3)	0	1/4	0.388(4)
O1	1.0	0.29485(5)	0.71842(5)	0.09651(5)	0.579(7)
O2	1.0	0.15990(5)	0.55480(5)	0.05381(5)	0.607(7)
O3	0.947(5)	0.44271(7)	0.36023(7)	0.02146(7)	0.65(1)
Si2	0.047(4)	1/2	1/4	1/8	0.6(2) *
H3	0.95	0.433(2)	0.354(2)	0.080(3)	4.6(7) *
O3A	0.044	0.456(2)	0.346(2)	0.036(2)	0.79 *
			8.6 GPa (space group *I4$_1$/acd*)		
Mn1	1.0	0	0	0	0.86
Ca1	1.0	0.36427(39)	0	1/4	0.98
Ca2	1.0	0	1/4	1/8	0.99
Si1	0.947	0.11789(48)	0	1/4	0.74(12) *
O1	1.0	0.29942(69)	0.71776(58)	0.09575(53)	0.91(13) *
O2	1.0	0.15909(68)	0.55218(61)	0.05617(67)	0.86(13) *
O3	1.0	0.44546(65)	0.35596(68)	0.02735(67)	0.76(14) *
Si2	0.047	1/2	1/4	1/8	0.8 *
H3	0.95	0.433	0.354	0.08	5.0 *
			293 K after heating excursion to 800 K (space group *Ia3d*)		
Mn1	1.0	0	0	0	1.33(5)
Mn2	0.044(5)	0.312(2)	0.062(2)	3/8	0.79
Ca	1.0	0	1/4	1/8	1.42(8)
Si1	0.81(2)	3/8	0	1/4	0.9(2)
O	1.0	0.4627(5)	-0.0487(5)	0.1540(5)	2.0(2)

Notes: B_{eq} values flagged * with standard deviation were refined isotropically, those without standard deviation were fixed.
For 100 and 293 K data: $B_{eq} = 8/3 \pi^2 \Sigma_i (\Sigma_j (U_{ij} a_i^* a_j^* a_i \bullet a_j))$; for 8.6 GPA data: $B_{eq} = 4/3 (\beta_{11} a^2 + \beta_{22} a^2 + \beta_{33} c^2)$.
† With 0.033 Al.

DISCUSSION

Structural features

Mn^{3+} in henritermierite displays a characteristic Jahn-Teller distortion of the tetragonally elongated type. The octahedron is built by the short axes O1-Mn-O1 and O3-Mn-O3 with Mn-O distances of 1.95 and 1.90 Å, respectively. The third axis O2-Mn-O2 is elongated with a Mn-O distance of ca. 2.2 Å. The reduced bond valence at O2, due to the expanded Mn-O2 distance (Table 8), is balanced by a shortened Si-O2 distance and by accepting a moderate hydrogen bond O3-H3···O2 (Fig. 3). Thus, the hydrogarnet substitution is favorable to the ordered Jahn-Teller distortion. Specifically, 1/3 of the oxygen atoms in henritermierite form weak Mn-O bonds and are privileged to accept an additional hydrogen bond which is the reason for the stoichiometry Ca$_3$Mn$_2^{3+}$[SiO$_4$]$_2$[H$_4$O$_4$] with the [SiO$_4$]/[H$_4$O$_4$] ratio of 2/1. The H$_4$O$_4$ tetrahedron, formed by O3 and H3, with a vacant center is very similar to the corresponding tetrahedron in Si-free katoite, Ca$_3$Al$_2$[H$_4$O$_4$]$_3$ (Lager et al. 1987). The distance from the center of the tetrahedron to O3 is 1.974

Å at 100 K [1.948 Å in Ca$_3$Al$_2$[H$_4$O$_4$]$_3$ (Lager et al. 1987)] and the protons are located slightly above the tetrahedral faces at a distance of 0.75 Å from O3. These empty tetrahedra behave as soft units and the center-to-O distance increases upon heating from 100 to 293 K by 0.008 Å (Table 6) and decreases at 8.6 GPa by 0.13 Å to 1.845 Å which probably depends on the strength or the dynamic character of the hydrogen bonds discussed below. The short O3-H3 distance of only 0.75 Å is characteristic of X-ray data on crystals with weak hydrogen bonds (Lager et al. 1987). The H position determined by X-ray diffraction reflects the position of the bonding electron between O and H. Additional O-H shortening, relative to the ideal value of about 1 Å, is expected for H librational disorder.

If the structure of henritermierite is viewed parallel to the *c*-axis (Fig. 4), endless open channels built by vacant H$_4$O$_4$ tetrahedra are visible along [001]. The tetragonal structure gives rise to two symmetrically independent Ca sites both eight-coordinated as in other garnets. However, Ca1 displays a very regular coordination with Ca-O distances between 2.44 and 2.47 Å [less distorted than in hydrous andradite (Armbruster 1995)

TABLE 6. Selected interatomic distances (Å) for henritermierite at 100 K, 293 K and compared with literature data, as well as bond distances at 8.6 GPa

		100 K	293 K	Aubry et al. (1969)	8.6 GPa
Mn-O3	2×	1.903(1)	1.904(1)	1.90(2)	1.900(8)
Mn-O1	2×	1.950(1)	1.952(1)	1.97(2)	1.941(6)
Mn-O2	2×	2.202(1)	2.206(1)	2.13(2)	2.139(8)
(Mn-O3A)	2×	2.02(5)	2.04(3)		
Si1-O2	2×	1.630(1)	1.630(1)	1.62(2)	1.612(9)
Si1-O1	2×	1.658(1)	1.657(1)	1.62(2)	1.643(7)
(Si2-O3A)	4×	1.75(4)	1.70(2)		
(Si2-O3)	4×	1.974(1)	1.982(1)		1.845(8)
Ca1-O3	2×	2.443(1)	2.445(1)	2.38(2)	2.425(8)
Ca1-O2	2×	2.444(1)	2.450(1)	2.43(2)	2.370(8)
Ca1-O2	2×	2.445(1)	2.451(1)	2.52(2)	2.398(9)
Ca1-O1	2×	2.472(1)	2.476(1)	2.45(2)	2.405(9)
(Ca1-O3A)	2×	2.63(4)	2.66(3)		
Ca2-O3	4×	2.333(1)	2.334(1)	2.33(2)	2.296(8)
Ca2-O1	4×	2.605(1)	2.614(1)	2.62(2)	2.494(7)
(Ca2-O3A)	4×	2.28(4)	2.33(3)		
O3-H3			0.75(3)	0.71(4)	0.635(8)
O2-H3			2.21(3)	2.23(3)	2.179(8)
O3-O2			2.763(1)	2.772(1)	2.691(11)
O3-O3	2×	3.287(2)	3.301(1)		3.068(11)
O3-O3			3.095(2)	3.103(1)	2.898(12)
O3-H3-O2		131(2)°	134(3)°		139.0(8)°
O3-H3-O3		141(2)°	138(3)°		134.1(8)°

Note: O3A and Si2 are low-occupied positions and only occur if O3 and H3 are vacant.

TABLE 7. Selected interatomic distances for dehydrated and oxidized henritermierite at 293 K (after heating excursion to 800 K)

Mn1-O	6x	2.009(5)	Si-O	4x	1.683(6)
Mn2-O	2x	1.87(2)	Ca-O	4x	2.362(6)
Mn2-O	2x	2.166(6)	Ca-O	4x	2.507(6)
Mn2-O	2x	2.15(3)			

Note: Mn2 is only occupied if two neighboring Si sites are vacant

TABLE 8. Bond valence calculations (Brown 1996) for henritermierite at 100 K

	Si	(Si2)	Mn	Ca1	Ca2	Σ
O1	0.953[2↑]		0.598[2↑]	0.255[2↑]	0.178[4↑]	1.984
O2	1.027[2↑]		0.303[2↑]	0.275[2↑]		1.880
				0.275[2↑]		
O3			0.679[2↑]	0.276[2↑]	0.372[4↑]	1.321
(O3A)		0.8[4↑]	0.5[2↑]	0.17[2↑]	0.35[4↑]	1.82
Σ^{O3}	3.960		3.160	2.162	2.200	
Σ^{O3A}	3.960	3.2	2.802	1.95	2.11	

Note: for stoichiometric henritermierite Si2 and O3A are vacant

TABLE 9. Henritermierite difference displacement parameters calculated along the bonding vector Me-O: $\Delta U_{Me-O} = (U_{Me} - U_O)$

T (K)	100	293
Si-O	−0.0002(3)	−0.0004(3)
Mn-O	−0.0014(3)	−0.0008(3)
Ca1-O	−0.0015(3)	−0.00016(3)
Ca2-O (mean)	−0.0007(3)	+0.0004(3)
Ca2-O3 (2.3 Å)	−0.0008(3)	−0.0002(3)
Ca2-O1 (2.6 Å)	−0.0006(3)	+0.0010(3)

and in $Ca_3Al_2[H_4O_4]_3$ (Lager et al. 1987)], whereas Ca2 has four Ca-O distances of 2.3 Å and additional four of 2.61 Å (considerably more distorted than in hydrous andradite and $Ca_3Al_2[H_4O_4]_3$). Difference displacement parameters (Table 9) are very similar to those determined for end-member andradite (Armbruster and Geiger 1993) indicating rigid vibrational behavior for SiO_4 and MnO_6 entities. ΔU(Ca2-O) increases with temperature indicating an anisotropic "rattling motion" of softly bound Ca.

Henritermierite may have a higher $[SiO_4]/[H_4O_4]$ ratio than 2/1 as derived from the idealized formula. The slightly Si-enriched sample has apparently additional Si in the center of the $[H_4O_4]$ tetrahedron. To balance the disordered arrangement, O3 splits into a second position O3A which is close (1.6–1.7 Å) to Si2 in the center of the tetrahedron. Due to the low Si2 occupancy in the present study, O3A could only be determined with low accuracy. Tables 6 and 8 indicate that occupation of O3A instead of O3 has only a minor effect on the distortion of the tetragonal structure. One may argue that for Si-rich varieties O2 can not balance the Jahn-Teller Mn-O2 elongation by forming a weak hydrogen bond. This could mean that in the neighborhood of Si2 the octahedra have a disordered Jahn-Teller distortion as found for $Mn_3Mn_2[SiO_4]_3$ (Arlt et al. 1998) and suspected for $Ca_3Mn_2[SiO_4]_3$ (Nishizawa and Koizumi 1975).

There are significant differences between the two known garnet structures with ordered Mn^{3+} Jahn-Teller distortion, synthetic $Ca_3Mn_2^{3+}[GeO_4]_3$ and henritermierite $Ca_3Mn_2^{3+}[SiO_4]_2$
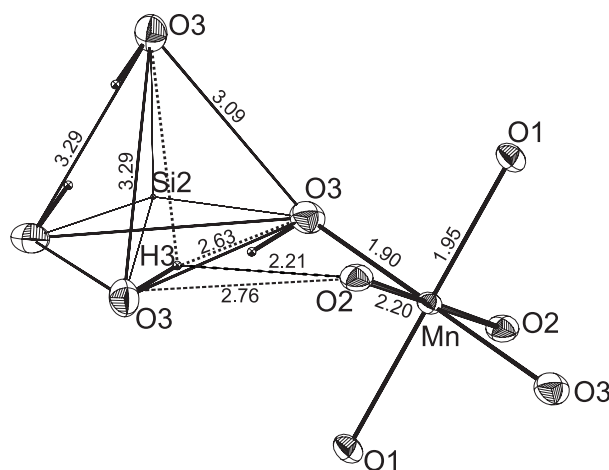

FIGURE 3. Hydrogen bonding in henritermierite showing the connectivity between the H_4O_4 tetrahedron and the MnO_6 octahedron (O, and Mn atomic displacement ellipsoids indicate 80% probability of the 100 K refinement; arbitrary size for H and Si2). Si2 is only locally occupied (4%) if the H positions are empty. The H site is positioned slightly above the tetrahedral faces and is hydrogen bonded to O2 and O3. The direction O2-Mn-O2 is Jahn-Teller elongated, thus O2 becomes slightly underbonded making O2 to an ideal acceptor of a moderate hydrogen bond. Numbers refer to distances in angstroms.

TABLE 10. Variation of the unit-cell parameters of henritermierite, $Ca^{2+}_3Mn^{3+}_2[SiO_4]_2[H_4O_4]$, with pressure
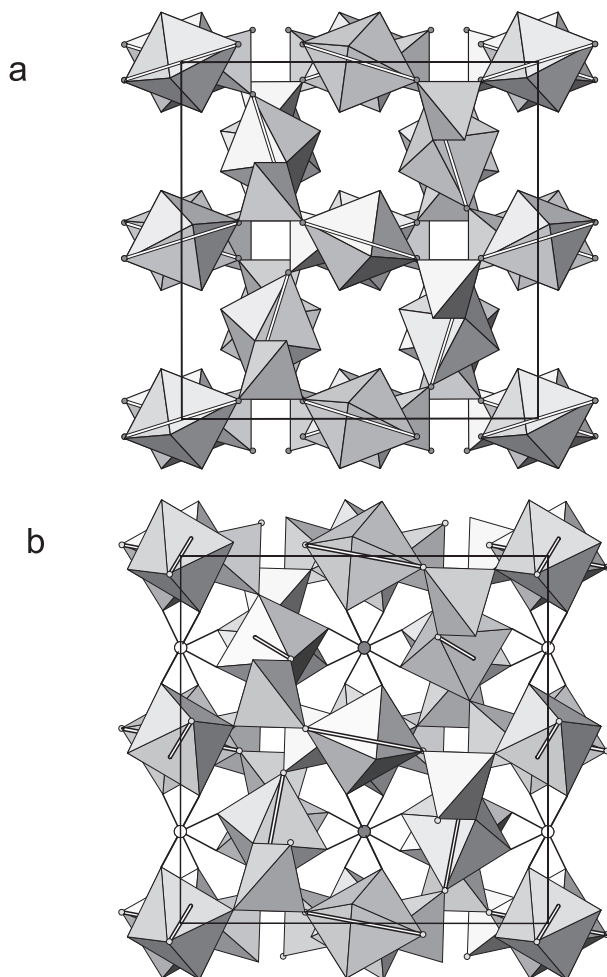
P (GPa)	Quartz		Henritermierite			
	V (Å³)	N_{refl}	a (Å)	c (Å)	V (Å³)	N_{refl}
			First data set			
0.0001*	113.090(21)	4	12.4938(6)	11.9120(8)	1859.42(18)	26
2.007(10)	107.900(14)	7	12.4016(6)	11.8548(8)	1823.28(19)	29
2.861(9)	106.109(12)	8	12.3654(5)	11.8316(7)	1809.09(17)	26
3.774(10)	104.389(13)	7	12.3300(5)	11.8083(7)	1795.20(16)	27
6.008(9)	100.812(9)	8	12.2473(5)	11.7517(7)	1762.71(17)	27
6.895(10)	99.583(9)	9	12.2158(5)	11.7294(7)	1750.33(16)	25
			Second data set			
0.0001*	113.099(21)	11	12.4871(6)	11.9107(9)	1857.22(21)	28
0.312(9)	112.175(16)	10	12.4729(7)	11.9023(9)	1851.68(22)	24
0.999(8)	110.309(11)	11	12.4409(6)	11.8822(8)	1839.08(20)	26
2.086(11)	107.735(18)	10	12.3936(7)	11.8521(10)	1820.50(24)	27
4.256(11)	103.557(14)	10	12.3055(9)	11.7951(11)	1786.08(29)	27
4.829(13)	102.610(18)	8	12.2858(11)	11.7819(15)	1778.37(34)	23
5.539(17)	101.508(24)	10	12.2585(7)	11.7629(9)	1767.61(23)	29
6.787(13)	99.736(15)	11	12.2170(6)	11.7335(7)	1751.28(19)	27
7.113(12)	99.303(13)	10	12.2064(6)	11.7262(8)	1747.16(20)	27
7.246(12)	99.130(13)	11	12.2013(6)	11.7224(7)	1745.14(18)	26
7.902(10)	98.299(8)	14	12.1797(7)	11.7085(10)	1736.88(22)	26
8.600(16)	[96.405(6) †	15]	12.1577(6)	11.6919(8)	1728.16(18)	26
8.701(17)	[96.321(14) †	16]	12.1542(6)	11.6903(8)	1726.94(18)	25

Note: Pressures determined from unit-cell volumes of quartz internal diffraction standard by applying the EOS of Angel et al. (1997).
N_{refl} = number of reflections used for the vector least-squares refinement of the unit-cell parameters.
* Crystal in DAC without pressure transmitting medium; V_0 used for equation of state.
† Not used for pressure determination.

[H_4O_4]. In henritermierite (space group $I4_1/acd$) the elongated O2-Mn-O2 axes lie essentially in the (001) plane (Fig. 4). This is the reason for the strong tetragonal distortion of the unit cell where *a* is approximately 0.55 Å larger than *c*. A difference of 0.48 Å was found for henritermierite from Tachgagalt which has ca. 25% Al on the octahedral site (Aubry et al., 1969). In contrast, $Ca_3Mn^{3+}_2[GeO_4]_3$ (space group $I4_1/a$) has two symmetry independent octahedral sites which show different orientations of the Jahn-Teller elongated axes (Fig. 4). One Mn site distorts the same way as in henritermierite but the second Mn site has the elongated axis preferentially oriented parallel to [001]. This more isotropic distribution of elongated O-Mn-O axes leads to a very weak distortion of the unit-cell dimension where *a* is less than 0.05 Å larger than *c*. The degree of distortion of individual $Mn^{3+}O_6$ octahedra is very similar in both structures. The more anisotropic bulk behavior of henritermierite is due to the cooperative effect of hydrogen bonding and Jahn-Teller distortion.

FIGURE 4. (**a**) Polyhedral model of the henritermierite structure (space group $I4_1/acd$) projected along the *c*-axis. Only SiO_4 tetrahedra and MnO_6 octahedra are shown. The open channels parallel to the *c*-axis host the H_4O_4 tetrahedra. The orientation of the Jahn-Teller elongated O2-Mn-O2 axes is shown by white lines. (**b**) Polyhedral model of the $Ca_3Mn_2[GeO_4]_3$ structure (space group $I4_1/a$) projected parallel to the *c*-axis (Heinemann and Miletich 2000). For better comparison with henritermierite, two tetrahedral Ge sites (open and filled circles) are connected by single lines with the four neighboring O positions and only one Ge site is shown as tetrahedron. Notice the different orientation of the Jahn-Teller elongated O-Mn-O axes compared to henritermierite.

Hydrogen bonding

The IR absorption bands between 3350 and 3600 cm^{-1} can be unambiguously assigned to the OH stretching modes of the H$_4$O$_4$ units in the henritermierite structure. Garnets without even traces of hydrogen do not show any absorption bands in this region, even in much thicker slabs (e.g., Bell and Rossman 1992). Garnets with hydrogarnet substitution (e.g., hydrogrossular) display two closely spaced intense bands around 3600 cm^{-1} (Rossman and Aines 1991). Compared to these bands, the 3432(5) cm^{-1} band in henritermierite occurs at rather low energies. This behavior is caused by enhanced hydrogen bonding in the structure. Whereas O-H···O distances in hydrogrossular amount to more than 3 Å, the distorted MnO$_6$ octahedra provide a much closer hydrogen-bond acceptor (O2) at a distance of only 2.76 Å. Because of the close distance of a hydrogen-bond acceptor, the O-H bond is slightly lengthened (and weakened) and consequently the stretching frequency is shifted towards lower wavenumbers. According to the stretching frequency-distance correlation of Mikenda (1986) an O···O distance of ca. 2.88 Å is expected from the band at 3432(5) cm^{-1}. This value deviates from the results of the X-ray investigation by ~0.12 Å. However, it must be taken into consideration that Mikenda (1986) used only well defined, straight (i.e., 180°) hydrogen bonds for his correlation, whereas the hydrogen bonds in henritermierite are considerably bent (angle O-H···O = 131°). Hence the effective H···O bond (the attractive force acting at the H position) is longer than in a straight bond and thus weaker than suggested by the short O···O distance. A recent frequency-distance correlation by Libowitzky (1999), who used a large number of mineral hydrates and hydroxides without any constraints on hydrogen-bond angles, gives much better agreement with an expected O3···O2 distance of 2.82 Å for the band at 3432(5) cm^{-1}. A structure refinement with a distance restraint of O-H = 0.98(1) Å resulted in an (apparent) H···O2 distance of 2.06 Å. In contrast, H···O vs. frequency correlations propose shorter H3···O2 distances of 1.94 Å (Mikenda, 1986) and 1.95 Å (Libowitzky, 1999) indicating a straighter hydrogen-bond configuration. This spectroscopic result may be best explained by a dynamic behavior of the H atom approaching (by a hopping motion) either the O2 or O3 hydrogen-bond acceptors (see also below). The weak dynamic disorder is resolved only by the fine time resolution of IR spectroscopy, whereas X-ray diffraction yields an average (apparently static) H atom position.

The relative intensities of the bands in the **E ∥ c** and **E ⊥ c** spectra provide further details of the O-H configuration. Because the O-H vectors in the H$_4$O$_4$ units of the henritermierite structure are oriented parallel to the *c*-axis rather than to the *a*-axis, the intensity of the band in the **E ∥ c** spectra is higher than in the **E ⊥ c** spectra. A more quantitative approach, however, using the relations of Libowitzky and Rossman (1996) yields an O-H angle of ~30° towards the *c*-axis, whereas the value from the X-ray structure determination is ~17°. This may be explained either by a dynamic behavior of the H atoms, e.g., by librational or hopping motion between the O2 and O3 hydrogen-bond acceptors, or by inaccurate intensities of the spectra which were slightly truncated at higher absorbance values. However, it must be emphasized that only the former explana-

tion of dynamic hydrogen-atom behavior is in perfect agreement with the frequency vs. distance correlations discussed above. In addition, a dynamic O-H orientation towards the remote O3 hydrogen-bond acceptors (O3-H···O3 = 3.29 Å, similar to hydrogrossular, e.g., Lager et al. 1987), may be also a reason for the additional side bands at 3508(2) and 3553(2) cm^{-1}, which occur predominantly in the **E ∥ c** spectra. However, the bands may be also caused by a slightly different crystal chemical environment, e.g., additional SiO$_4$ tetrahedra instead of neighboring H$_4$O$_4$ units, which shift the IR bands to higher wavenumbers either by cationic effects, or by distortion of the H bond, i.e., towards a more bent or longer O-H···O bond. The relatively constant wavenumber with changing temperature is in agreement with the general behavior of weak to moderate H bonds (Lutz 1995). Additional trace-hydrogen incorporation at different structural sites similar to that in common garnets (Bell and Rossman 1992) may be suspected, the respective trace-absorption bands, however, cannot be observed in a platelet of only 10 μm thickness.

High-pressure behavior

The study of OH-bearing henritermierite under high pressure is of high interest as garnets are assumed to be possible hosts for storage of water in the Earth's upper mantle. Stability and properties of minerals under these extreme conditions depend strongly on the chemical composition. The comparison of henritermierite with other Mn^{3+}- or OH-bearing garnets reveals the effects of H$_4$O$_4$ ↔ SiO$_4$ substitution and of Jahn-Teller distortion on the pressure derived properties. The compressibility of henritermierite ($K_{0,T}$ = 97.9(9) GPa, K' = 5.3(3)) is higher by about 1/3 compared to OH-free Mn^{3+}-bearing garnets, such as Mn$_3^{2+}$Mn$_2^{3+}$[SiO$_4$]$_3$ with a bulk modulus of K_0 = 151.6(8) GPa and its pressure derivative of K' = 6.38(19) (Arlt et al. 1998). Miletich et al. (1997) found data of K_0 = 133.0(6) GPa, K' = 5.7(2) for Ca$_3$Mn$_2^{3+}$[GeO$_4$]$_3$. Spessartine, Mn$_3$Al$_2$[SiO$_4$]$_3$, was measured to show data of K_0 = 171.8(1.6) GPa, K' = 7.4(1.0) or K_0 = 174.2(1.6) GPa, K' = 7.0(1.0) (Babuska et al. 1978; Leger et al. 1990). The bulk modulus systematics clearly indicate the degree of hydrogarnet substitution to be the dominant factor for the overall compressional behavior. In accordance with that, the fully deuterated hydrogarnet katoite, Ca$_3$Al$_2^{3+}$[D$_4$O$_4$]$_3$, with a bulk modulus of K_0 = 52(1) GPa (Lager and von Dreele 1997), is almost twice as compressible as henritermierite. The high value for K' in henritermierite is similar to those in other Mn^{3+} garnets. It is attributed to the changes of electronically induced polyhedral distortion at high pressures (Arlt et al. 1998; Woodland et al. 1999). The comparison of the axial bulk moduli indicates a compressional axial anisotropy of henritermierite (Fig. 5), which is in contrast to the quasi-isotropic behavior found in tetragonal Ca$_3$Mn$_2^{3+}$[GeO$_4$]$_3$ (Miletich et al. 1997). The distinct differences in the orientation of the axis of polyhedral elongation explain the higher axial compression along the [100]$_{tetr}$ directions compared to that along the *c*-axis. This hypothesis is confirmed by the structural behavior at high pressure. The elongated Mn-O2 bond distance of the Jahn-Teller distorted MnO$_6$ octahedra in [100]$_{tetr}$ directions (2.206 Å at ambient conditions) is shortened much more (Mn-O2 = 2.139 Å at 8.6 GPa, Δ = 0.067 Å) compared to dif-
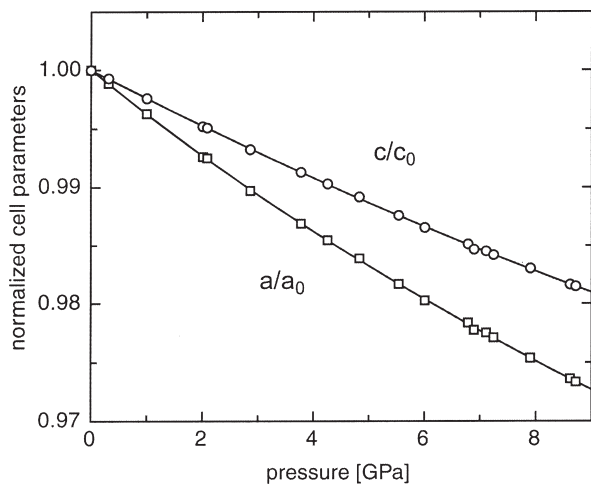
FIGURE 5. Anisotropic behavior of cell parameters of henritermierite as a function of pressure.

ferences of only 0.004 and 0.011 Å for the other two octahedral bond lengths. This results in a more regular polyhedron at higher pressure. The anisotropic compression of the MnO_6 octahedron can be explained by the exponential relationship between bond lengths and bond valences. The stronger compression of the long bonds relative to short bonds leads to a smaller compressional overbonding on the atoms involved for a given volume reduction. In our example, the preferred compression of the long Mn-O2 bond reduces the overbonding for the Mn cation from 3.4 v.u. for an isotropic compression to 3.3 v.u. Compressional overbonding due to high pressure is thus acting against the Jahn-Teller distortion due to the energetic degeneracy of the d-orbitals. Major structural changes are also observed for the Ca polyhedra. Eight-fold coordinated Ca fills the large cavities of the corner-sharing tetrahedral and octahedral framework. In agreement with bond-valence considerations the very long Ca2-O1 bond (2.614 Å at ambient conditions) is affected strongest within the Ca2 polyhedron, which shows a tendency towards a more regular shape. We also observe a remarkable reduction of the O3-O3 distance. This results in an apparent strengthening of the O3-H3···O3 hydrogen bond. This observation should however be interpreted with caution, because the quality of the high-pressure data set did not allow us to refine the hydrogen position.

Both the c/a ratio and spontaneous strain (Fig. 6) show a trend towards a weaker tetragonal distortion at high pressures. On the basis of this trend we expect pseudo-cubic cell dimensions above ca. 20 GPa but the structure will still be tetragonal due to the ordered distribution of SiO_4 and H_4O_4 tetrahedra.

Dehydration and oxidation behavior

The first dehydration experiments on henritermierite were performed by Gaudefroy et al. (1969) using differential thermal analysis (DTA) and thermal gravimetry (TG), which showed an endothermic reaction starting at ca. 750 K accompanied by weight loss of ca. 4 wt%. At 910 K an exothermic reaction started that had its maximum at 1100 K. The total weight loss at 1100 K was 8.7%. Considering that this
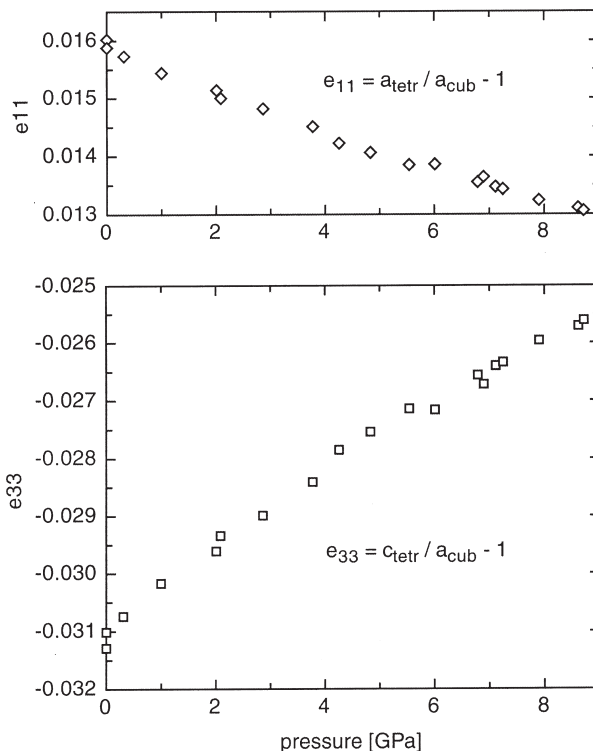

FIGURE 6. Strain calculated from cell parameters for a tetragonal to cubic cell. "a_{cub}" is the hypothetical cubic cell parameter corresponding to the given cell volume.

Tachgagalt sample had 7.85 wt% H_2O, probably additional O_2 was released due to partial reduction of Mn_2O_3 to MnO. After this heating excursion (the maximum temperature was 1300 K) an X-ray powder pattern was recorded displaying garnet and braunite reflections. Unfortunately the authors do not report whether their dehydration experiments were performed in air or under inert gas. In air, low temperature oxidation of Mn^{3+} to Mn^{4+} must be expected (Kohler et al. 1997), whereas under low oxygen fugacity only high-temperature reduction of Mn^{3+} to Mn^{2+} may be predicted.

Our single-crystal dehydration experiments in air yielded at ~750 K a cubic garnet-like phase that remained stable after slow cooling to room temperature. The observation that the X-ray reflections became strongly streaked and decreased in intensity compared to the original henritermierite diffraction pattern indicates that an additional X-ray amorphous phase was produced during this reaction. Derived from the refined composition of the garnet-like phase, the dehydration-oxidation reaction of henritermierite may be expressed as: $Ca_3Mn_2[SiO_4]_{2.07}[H_4O_4]_{0.93} + 0.32\ O_2 \rightarrow 0.85\ Ca_3Mn_{2.26}O_{2.32}$ $[SiO_4]_{2.42} + 0.07\ MnO_2 + 0.44\ CaO + 1.86\ H_2O$. Observation of cubic symmetry for the new garnet-like phase suggests (1) that the ordered distribution of H_4O_4 entities was lost because H_2O was expelled and (2) that the new phase no longer exhibits an ordered Jahn-Teller distortion. The structure of dehydrated henritermierite has significantly more SiO_2 than the starting material, 2.42(6) SiO_4 pfu versus 2.07 SiO_4 pfu. Thus the dehydrated garnet-like phase has only 0.58(6) tetrahedral vacan-

cies pfu. In addition, we located a new octahedral Mn2 site (Fig. 7) between two neighboring tetrahedral positions. Site occupation refinements led to 0.26(3) Mn pfu on this new site. The numerical relationship (2/1) of tetrahedral vacancies and occupied Mn2 sites indicates short range ordering: Mn2 can only be occupied if two adjacent tetrahedral sites are vacant. This relation also indicates that the new garnet-like phase can not have H_4O_4 tetrahedral entities. Furthermore, the structure refinement led to the composition $Ca_3Mn_{2.26}O_{2.32}[SiO_4]_{2.42}$, suggesting that the average valence of Mn is 3.68. The increased Si-O distance of 1.683(6) Å and the distorted octahedral coordination of Mn2 are a consequence of the disordered character of the structure. Assumption of a strongly disordered structure is also corroborated by the increased displacement parameters (Table 5). The refined composition and the X-ray scattering behavior of the new garnet-like phase requires that due to dehydration and oxidation of henritermierite at least one additional, coherently intergrown, Ca-enriched phase has formed. Thus a spectroscopic characterization or supporting electron microprobe analysis had to be abandoned. In general, the dehydration and oxidation behavior of henritermierite is similar to $Mn^{3+}OOH$ (groutite and manganite) for which Kohler et al. (1997) determined upon heating in air above 600 K a topotactic transformation to MnO_2, pyrolusite. Recently Li et al. (1998) reported dehydration of the synthetic hydrogarnet $Sr_3Fe_2^{3+}[H_4O_4]_3$ at 803 K in which simultaneously Fe^{3+} was oxidized to Fe^{4+}. However, the question whether the new anhydrous oxidized phase is of the garnet type was not addressed.

There are two constraints for the composition of the new garnet-like phase. (1) For steric reasons Mn on the new octahedral site (Mn2) requires two adjacent tetrahedral vacancies. (2) The incorporation of additional octahedral Mn is exhausted if all Mn^{3+} is oxidized to Mn^{4+}. This leads to the hypothetical limiting composition $Ca_3Mn_{2.5}^{4+}O_4[SiO_4]_2$. The observed composition of the new garnet-like phase is approximately halfway between $Ca_3Mn_2^{3+}[SiO_4]_3$ and the above-defined limiting stoichiometry.

REFERENCES CITED

Aines, R.D. and Rossman, G.R. (1984) The hydrous component in garnets: Pyralspites. American Mineralogist, 69, 1116–1126.

Amthauer, G., Katz-Lehnert, K., Lattard, D., Okrusch, M., and Woermann, E. (1989) Crystal chemistry of natural Mn^{3+}-bearing calderite-andradite garnets from Otjosondu, SWA/Namibia. Zeitschrift für Kristallographie, 189, 43–56.

Angel, R.J., Allan, D.R., Miletich, R., and Finger, L.W. (1997) The use of quartz as an internal pressure standard in high pressure crystallography. Journal of Applied Crystallography, 30, 461–466.

Arlt, T., Armbruster, T., Miletich, R., Ulmer, P., and Peters, T. (1998) High pressure single-crystal synthesis, structure and compressibility of the garnet $Mn_3^{2+}Mn_2^{3+}[SiO_4]_3$. Physics and Chemistry of Minerals, 26, 100–106.

Armbruster, T. (1995) Structure refinement of hydrous andradite $Ca_3Fe_{1.54}$ $Mn_{0.20}Al_{0.26}(SiO_4)_{1.65}(O_4H_4)_{1.35}$, from the Wessels mine, Kalahari manganese field, South Africa. European Journal of Mineralogy, 7, 1221–1225.

Armbruster, T. and Geiger, C.A. (1993) Andradite crystal chemistry, dynamic X-site disorder and structural strain in silicate garnets. European Journal of Mineralogy, 5, 59–71.

Armbruster, T. and Lager, G.A. (1989) Oxygen disorder and the hydrogen position in garnet-hydrogarnet solid solutions. European Journal of Mineralogy, 1, 363–369.

Armbruster, T., Birrer, J., Libowitzky, E., and Beran, A. (1998) Crystal chemistry of Ti-bearing andradites. European Journal of Mineralogy, 10, 907–921.

Aubry A., Dusausoy Y., Laffaille A., and Protas J. (1969) Détermination et étude de la structure cristalline de l'henritermierite, hydrogrenat de symétrie quadratique. Bulletin de la Societe Francaise de Minéralogie et de Cristallographie, 92, 126–133.

Babuska, V., Fiala, J., Kumazawa, M., Ohno, I., and Sumino, Y. (1978) Elastic properties of garnet solid solution series. Physics of the Earth and Planetary Interiors, 16, 157–176.

Bell, D.R. and Rossman, G.R. (1992) The distribution of hydroxyl in garnets from the subcontinental mantle of southern Africa. Contributions to Mineralogy and Petrolology. 111, 161–178.

Blessing, R.H. (1987) Data reduction and error analysis for accurate single crystal diffraction intensities. Crystallography Reviews, 1, 3–58.

Brown, I.D. (1996) VALENCE: a program for calculating bond valences. Journal of Applied Crystallography, 29, 479–480.

Bühn, B., Okrusch, M., Woermann, E, Lehnert, K., and Hoernes, S. (1995) Metamorphic evolution of neoproterozoic manganese formations and their country rocks at Otjosondu, Namibia. Journal of Petrology, 36, 463–496.

Burnham, C.W. (1966) Computation of absorption corrections and the significance of end effects. American Mineralogist, 51, 159–167.

Cairncross, B., Beukes, N., and Gutzmer, J. (1997) The Manganese Adventure; The South African Manganese Fields. Associated Ore and Metal Cooperation Limited. Marshalltown, Johannesburg 2107, Republic of South Africa, 236 p.

Creagh, D.C. and McAuley, W.J. (1992) X-ray dispersion correction. In A.J.C. Wilson, Ed., International tables for crystallography, vol C. Kluwer Academic Publishers, Dordrecht, 206–219.

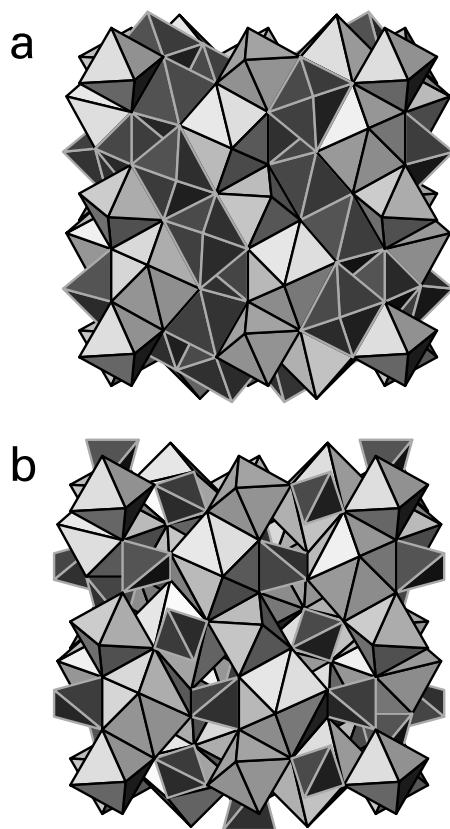Enraf Nonius (1983) Structure determination package (SDP). Enraf Nonius, Delft,

FIGURE 7. (a) Arrangement of Mn2 octahedra (dark with light rims) in the new garnet related phase. The multiplicity of the new Mn2 site is twice that of Si in regular garnets. Thus this polyhedral drawing displays all possible Mn2 sites. In the refined structure only one Mn2 pfu statistically replaces two adjacent Si sites. (b) Arrangement of SiO_4 tetrahedra (dark with light rims) in a regular garnet structure.

Holland.

Frentrup, K.R. and Langer, K. (1981) Mn^{3+} in garnets: Optical absorption spectrum of a synthetic Mn^{3+} bearing silicate garnet. Neues Jahrbuch für Mineralogie Monatshefte, 1981, 245–256.

Finger, L.W. and King, H.E. (1978) A revised method of operation of the single-crystal diamond cell and refinement of the structure of NaCl at 32 kbar. American Mineralogist, 63, 337–342.

Finger, L.W. and Prince, E. (1975) A system of Fortran IV computer programs for crystal structure computations. United States National Bureau of Standards, NBS Technical note, 854.

Gaudefroy, C., Orliac, M., Permingeat, F., and Parenoff, E. (1969) L'henritermiérite, une nouvelle espèce minérale. Bulletin de la Societe Francaise de Minéralogie et de Cristallographie, 92, 185–190.

Geiger, C.A., Stahl, A., and Rossman, G.R. (1999) Raspberry-red grossular from Sierra de Cruces Range, Coahuila, Mexico. European Journal of Mineralogy, 11, 1109–1113.

Grant, D.F. and Gabe, E.J. (1978) The analysis of single-crystal Bragg reflections from profile measurements. Journal of Applied Crystallography, 11, 114–120.

Heinemann, S. and Miletich, R. (2000) Structure and twinning of tetragonal Ca$_3$Mn$_2$(GeO$_4$)$_3$ garnet. American Mineralogist, 993–1000.

Henmi, C., Kusachi, I., and Henmi, K. (1995) Morimotoite, Ca$_3$TiFe^{2+}Si$_3$O$_{12}$, a new titanian garnet from Fuka, Okayama Prefecture, Japan. Mineralogical Magazine, 59, 115–120.

Holstam, D. and Hålenius, U. (1998) Mn^{3+}-bearing garnets and hydrogarnets. Abstracts and Programme, 17th General Meeting, International Mineralogical Association, Toronto, Canada, A-103.

King, H.E. and Finger, L.W. (1979) Diffracted beam crystal centering and its application to high-pressure crystallography. Journal of Applied Crystallography, 12, 374–378.

Kobayashi, S. and Shoji, T. (1987) Infrared spectra and cell dimensions of hydrothermally synthesized grandite-hydrograndite series. Mineralogical Journal, 13, 490–499.

Kohler, T., Armbruster, T., and Libowitzky, E. (1997) Hydrogen bonding and Jahn-Teller distortion in groutite, α-MnOOH, and manganite, γ-MnOOH, and their relation to the manganese dioxides ramsdellite and pyrolusite. Journal of Solid State Chemistry, 133, 486–500.

Lager, G.A. and von Dreele, R.B. (1996) Neutron powder diffraction study of hydrogarnet to 9.0 GPa. American Mineralogist, 81, 1097–1104.

Lager, G.A., Armbruster, T., and Faber, F. (1987) Neutron and X-ray diffraction study of hydrogarnet Ca$_3$Al$_2$(O$_4$H$_4$)$_3$. American Mineralogist, 72, 756–765.

Lager, G.A., Armbruster, T., Rotella, F.J., and Rossman, G.R. (1989) OH substitution in garnets. X-ray and neutron diffraction, infrared, and geometric modeling studies. American Mineralogist, 74, 840–851.

Langer, K. and Lattard, D. (1984) Mn^{3+} in garnets II: Optical absorption spectra of blythite-bearing, synthetic calderites, Mn$_3^{3+[8]}$(Fe$_{1-x}^{3+}$Mn$_x^{3+}$)$_2$$^{[6]}$[SiO$_4$]$_3$. Neues Jahrbuch für Mineralogie Abhandlungen, 149, 129–141.

Leger J.M., Redon, A.M., and Chateau, C. (1990) Compressions of synthetic pyrope, spessartine and uvarovite garnets up to 25 GPa. Physics and Chemistry of Minerals, 17, 161–167.

Li, G., Mao, Y., Li, X., Zhu, L., and Feng, S. (1998) Hydrothermal synthesis and Mössbauer spectra study of hydrogarnet Sr$_3$Fe$_2$(OH)$_{12}$ (in Chinese). Chemical Journal of Chinese Universities, 19, 1195–1199.

Libowitzky, E. (1999) Correlation of O-H stretching frequencies and O-H···O hydrogen bond lengths in minerals. Monatshefte für Chemie, 130, 1047–1059.

Libowitzky, E. and Rossman, G.R. (1996) Principles of quantitative absorbance measurements in anisotropic crystals. Physics and Chemistry of Minerals, 23, 319–327.

Lutz, H.D. (1995) Hydroxide ions in condensed materials—correlation of spectroscopic and structural data. Structure and Bonding, 82, 85–103.

Maslen, E.N., Fox, A.G., and O'Keefe, M.A. (1992) X-ray scattering. In A.J.C. Wilson, Ed., International tables for crystallography, vol C. Kluwer Academic Publishers, Dordrecht, 476–509.

Medenbach, O. and Shannon, R.D. (1997) Refractive indices and optical dispersion of 103 synthetic and mineral oxides and silicates measured by a small-prism technique. Journal of the Optical Society of America, B14, 3299–3318.

Mikenda, W. (1986) Stretching frequency versus bond distance correlation of O-D(H)···Y (Y = N, O, S, Se, Cl, Br, I) hydrogen bonds in solid hydrates. Journal of Molecular Structures, 147, 1–15.

Miletich, R., Armbruster, T., Heinemann, S., and Angel, R.J. (1997) Tetragonal garnets and Jahn-Teller effect: Influence of pressure and temperature on the cooperative distortion. EOS Transactions, AGU, 78, Supplement F754.

Nishizawa, H. and Koizumi, M. (1975) Synthesis and infrared spectra of Ca$_3$Mn$_2$Si$_3$O$_{12}$ and Cd$_3$B$_2$Si$_3$O$_{12}$ (B: Al, Ga, Cr, V, Fe, Mn) garnets. American Mineralogist, 60, 84–87.

Rossman, G.R. and Aines, R.D. (1991) The hydrous components in garnets: Grossular-hydrogrossular. American Mineralogist, 76, 1153–1164.

Sacerdoti, M. and Passaglia, E. (1985) The crystal structure of katoite and implications within the hydrogrossular group of minerals. Bulletin de Minéralogie, 108, 1–8.

Sheldrick, G.M. (1997) SHELXL-97 and SHELXS-97. Programs for crystal structure determination. University of Göttingen, Germany.

Woodland, A.B., Angel, R.J., Koch, M., Kunz, M., and Miletich, R. (1999) Equations of state for Fe$_3^{2+}$Fe$_2^{3+}$Si$_3$O$_{12}$ "skiagite" garnet and Fe$_2$SiO$_4$-Fe$_3$O$_4$ spinel solid solutions. Journal of Geophysical Research, 104, B9, 20049–20058.